Evolutionary rate incongruences in squamates reveal contrasting patterns of evolutionary novelties and innovation

Tiago R. Simões[1,4*], Arthur S. Brum[2] and Stephanie E. Pierce[3]

[1]Department of Ecology and Evolutionary Biology, Princeton University, Princeton-NJ, 08540, USA;

[2]Laboratório de Sistemática e Biogeografia, Departamento de Zoologia, Universidade do Estado do Rio de Janeiro, Rio de Janeiro, Rio de Janeiro 20940-040, Brazil;

[3]Museum of Comparative Zoology and Department of Organismic and Evolutionary Biology, Harvard University, Cambridge, MA 02138, USA.

[4]Lead contact

*Correspondence: simoes@princeton.edu

SUMMARY

Understanding the rate of phenotypic evolution can reveal fundamental aspects of organismal evolutionary trajectories. Hence, several studies have attempted to detect the tempo of evolution for multiple organisms, although based on radically different datatypes (e.g., discrete and morphometric) and methods (phylodynamic vs comparative methods). Here, we ask whether these competing approaches provide comparable rate trajectories using an expanded squamate phylogenetic dataset that is matched (to the species-level) with new geometric morphometric data, while also assessing method robustness to fossil sampling. Our new squamate total-evidence time-tree suggests a new placement for putative stem iguanians while matching divergence time estimates of recent phylogenomic studies. We show that low fossil sampling inadvertently removes entire regions of the morphospace and contraction of crown clade phenotypic diversity, as morphospace boundaries are frequently delimited by transitional fossils. Critically, different datatypes produce radically incongruent rate patterns, which are further exacerbated by methodological differences. We suggest that phylogenetic discrete data (i.e., characters) are strongly influenced by neomorphisms and reveal phenotypic novelties, while morphometric data (i.e., shape) reflects changes in phenotypic refinement leading to phenotypic innovation. This conceptual distinction conciliates discrepant macroevolution trajectories across squamates, which we expect to be generalizable to other systems across the Tree of Life.

Keywords: evolutionary rates; macroevolution; phylogenetic comparative methods; phylodynamics; squamates; morphospace

INTRODUCTION

Inferring rates of phenotypic evolution at macroevolutionary scales provide fundamental insights into the tempo of adaptive changes governing the origin of new body plans and other major evolution transitions across the tree of life[1-3]. Phenotypic rate inference has a long tradition in evolutionary biology and paleobiology[1,2], but it has undergone an overhaul over the last two decades due to the increasing availability of new data and quantitative phylogenetic tools[4-8]. The result has been a proliferation of studies that have provided insights into phenotypic macroevolutionary rate dynamics across various taxonomic and timescales[3,9-15]; thus inferring events of major phenotypic novelties and innovations[3,16-19], and their role in macroevolutionary phenomena such as adaptive radiations[3,17,18]. Further, evolutionary rate estimates can also be used to assess the mode and strength of natural selection across various subdivisions of the phenotype, and thus enabling such insights into extinct species for which molecular data is unavailable[20-22].

Despite these technical advances and new empirical implementations, important theoretical and practical differences in estimating evolutionary rates have historically remained uninvestigated. Recently, however, these have captured broader scientific interest, such as a suggested pervasive relationship between evolutionary rates and chronological branches lengths in evolutionary trees (i.e. time-trees), potentially biasing rate estimates[2,23], but which was subsequently demonstrated to be the result of mathematical[24,25] or taxon sampling artifacts[26]. From both a theoretical and practical perspective, another key aspect (but which has seldomly been explored) is whether different approaches to infer evolutionary rates produce comparable results and how they perform under different empirical conditions. If competing approaches do not produce comparable results, in which specific way do they differ from each other in terms of performance and usefulness to test different kinds of hypotheses?

The two main approaches of evolutionary rate inference for phenotypic data are phylodynamic methods (sensu Stadler *et al.* [4]) and phylogenetic comparative methods (PCM). Phylodynamic rate inference uses complex mechanistic models, including diversification and clock models, to jointly estimate phylogenetic trees and many evolutionary parameters, such as rates of phenotypic and/or molecular evolution, speciation, extinction, among others. PCM approaches, on the other hand, assume a (or a set of) fixed tree topology and map trait evolution

under a stochastic model, most commonly Brownian Motion[8]. Furthermore, phylodynamic approaches almost always take as input discrete data (e.g., as morphological characters, nucleotides, amino acids), whereas PCM can utilize both datatypes, although most studies have used continuous data, such as body mass or multivariate traits (e.g., obtained from geometric morphometrics—GMM). These approaches have been well-described in the evolutionary literature[4,7], and applied to several study systems over the past decade (e.g.,[3,12,14,15,27-31]), with important conclusions regarding their macroevolutionary trajectories, such as the timing and processes behind the origin of phenotypic novelties and innovations in fishes, early reptiles, squamates, non-avian dinosaurs, birds, and placental mammals [3,9-15,32].

Here, we apply phylodynamic and PCM methods for estimating the rate of phenotypic evolution, test their robustness, and impact on interpretations regarding the tempo, mode of selection, and patterns of phenotypic novelty and innovation for the largest group of terrestrial vertebrates on Earth today—squamates (lizards and snakes). Squamates have been the recent focus of attention in using phenotypic rates to identify major evolutionary novelties and innovations, using both phylodynamics and PCM methods [3,9,10,12,33]. These studies have produced radically different conclusions on their rates of evolution and inferred patterns of phenotypic change, making them the perfect study system to address the questions put forward herein. We start by substantially expanding a total-evidence phylogenetic dataset[3,34-38] of squamates and their closest lepidosaurian relatives (i.e., 60% taxonomic sampling increase, and 21% increase in morphological discrete characters). This dataset was used to produce a new time-calibrated tree of squamates and their kin, including ample sampling of both living and fossil species, that was used to infer phylodynamic rates of evolution. We complemented this by also collecting geometric morphometric (GMM) data on the same species—in fact, most of the data obtained from the same specimens. The latter was used for inferring evolution rates using the only two PCM methods that implement branch-by-branch evolution rate inference (thus comparable to phylodynamic inference) using multivariate data (BayesTraits[39] and RRphylo[40]). To our knowledge, this is the first time that rates of evolution based on phylodynamics and GMM data are directly compared to each other while including the fossil record.

Our results reveal a major discrepancy between clock-based phylodynamic and PCM rate inferences. Many of those differences are dependent on data type (i.e. discrete anatomical characters vs. continuous shape variables), with each data type providing answers to

ontologically different aspects of phenotypic evolution. Moreover, we find that the methods tested here vary greatly in robustness to fossil sampling, with the phylodynamic approach being more consistent than PCM methods. Further, BayesTraits was the least robust and with much greater disparity of rate estimates than either clocks or RRphylo, for all clades analyzed separately or together and regardless of fossil sampling effort. We conclude by proposing a conceptual complementarity between rate estimates using different data types and guidelines on how downstream conclusions can be obtained from each of them.

RESULTS

Total evidence time-tree of early lepidosaurs and squamates

The total-evidence dating (TED) phylodynamic analyses using a single morphological and a single molecular partition produced topological results and divergence times (Fig. 1a, Suppl. Fig. S1) that are broadly congruent with previous phylogenomic and TED studies[3,38,41]. Among the contending areas of discordance between previous phylogenomic and TED studies, and which are of greater relevance to broader squamate systematics, we find Dibamidae as the sister group to Unidentata—as in[42,43]—rather than at the earliest crown squamate clade[44] or as a sister to gekkotans[45]. We also find snakes as the earliest diverging toxicoferan clade along with Mosasauria, which has been a trend in several recent TED analyses, even when using highly distinct morphological data sets[3,38,41,46,47].

Among the placement of important fossil taxa, we highlight the recovery of the fossil taxa *Palaeagama, Taytalura, Sophineta,* and *Fraxinisaura* as stem lepidosaurs and great uncertainty in the relationships among the stem fossil squamates *Bellairsia, Oculudentavis,* and *Huhuecuetzpalli*. The latter, instead of being recovered as stem squamates as in recent studies[41,48], are inferred herein as early diverging taxa within crown squamates—forming a sister clade to gekkotans (although with very low support). We find great uncertainty surrounding the internal relationships within early diverging mosasaurians, but we recover a monophyletic Dolichosauridae (inclusive of the once-proposed "four-legged snake" *Tetrapodophis*, supporting recent findings[49]) and a strongly supported clade formed by *Aigialosaurus* and mosasauroids. Contrary to all previous squamate trees inclusive of fossil taxa, we find most iguanians from the Late Cretaceous of Mongolia (except for *Saichangurvel*) as sister taxa to acrodontans, instead of

their traditionally placement as part of an early pleurodontan radiation (e.g.,[50,51]), This is driven by many (and previously overlooked) similarities between these (specially *Ctenomastax*) and acrodontans regarding their mode of tooth attachment (see Suppl. Fig. S2).

Divergence time estimates are broadly consistent with previous TED and phylogenomic results. This is true for the time of origin for total group Squamata—252.5 Ma herein, and 250.3 Ma in Simões *et al.* [3]—and for crown group Squamata—214.6 Ma herein and in the most recent phylogenomic time-tree by Title *et al.* [9] at 213.2 Ma (Norian, Late Triassic). Both results also push back the crown age relative to most other previous estimates, which were between 186 and 206 Ma[3,45,52,53]. Agreement with recent results is also found for Unidentata—194 Ma herein, and between 189.5 to 203.7 Ma (latest Triassic to Early Jurassic,) in most previous TED and phylogenomic studies[3,45,46,52] (except for 176 Ma in [46]). Toxicofera is found to have originated at 182.6 Ma herein and between 170 to 184.6 Ma (Toarcian-Aalenian; Early-Middle Jurassic) in previous studies[3,45,46,52,53]. These results demonstrate an increasing consensus on age estimates for the deepest nodes on the squamate tree of life, despite using radically different datasets and dating methods. Notably, these results are also consistent across different iterations of this same dataset, despite changes in taxonomic sampling and placement of some fossils, thus providing empirical support to recent theoretical work suggesting that uncertainty in fossil placement does not significantly impact the accuracy of divergence time estimates[54].

Morphospace occupation and the impact of fossil sub-sampling

Using GMM data from the dorsal skull surface, we tested changes in morphospace occupation for each clade while systematically reducing the total number of fossil taxa in the dataset (from 24.5%, to 14%, then to 0%). The results (Fig. 1b-d, Suppl. Fig. S3) indicate that, for all PC comparisons, reduction in fossil sampling creates two main effects. The first, as expected, is that fossil removal generates the disappearance of regions of the morphospace that are exclusively occupied by extinct clades—e.g., upper right quadrant in Fig. 1b is occupied by fossil sphenodontians and stem lepidosaurs only. We considered this to be a Type II bias in morphospace representation—a false indication of unoccupied areas of the morphospace that are in fact occupied.

Second, the edges of the morphospace occupied by crown squamate families are frequently delimited by fossils taxa—e.g., polyglyphanodontians for Lacertoidea; stem fossil

snakes for early snakes ("Haenophidia") (Fig.1b). Therefore, iterative fossil removal contracts crown clade morphospaces (Figs. 1b-d, Suppl. Fig. S3). This can be explained by the fact that early fossil members of a clade should present a suit of plesiomorphic and derived phenotypes, which in practice, represent transitional body plans between crown clades. This pattern is most likely not exclusive to squamates and might represent a generalizable property of low fossil sampling that should also be expected for other groups. Importantly, however, we find that the relative positions of crown clade morphospaces are almost unaffected even by complete removal of fossils (Figs 1b-d, Suppl. Fig. S3). This indicates that even studies focusing on extant taxonomic sampling for squamates, or with low fossil sampling (e.g., [9,12]), are still able to provide an accurate depiction of relative morphospace occupation of their main respective sub-clades.

Clock rates across clades and morphological partitions

Our TED phylodynamic inference applying multiple morphological clocks for all sampled species and across morphological partitions of the squamate phenotype revealed an interesting mosaic of rates of change across body regions (Fig. 2a-d). This approach enables a more detailed assessment of the mosaic of rate patterns across the phenotype than inferring rates for the phenotype as a whole, such as a single "global morphological clock" (Suppl. Fig. S4). For instance, phenotypic rates are slower on mandibles, dentition and postcranial characters relative to skull surface, palate and braincase (Fig. 2e). Additionally, the fast rates of evolution detected in the earliest branches leading up to early snakes and scolecophidians (blind-snakes) using a global morphological clock (Suppl. Fig. S4) are detected here as driven by fast rates of change across many body subdivisions, but proportionately less by mandibular and dentition characters (Fig. 2c). In amphisbaenians (worm-lizards), we see a global pattern of accelerated rates early in their evolution, which partitioned clocks revealed to be mostly driven by high rates of change in the palate and braincase, and postcranial partitions, with proportionately much slower rates in skull surface, or in their mandible and dentition. Faster rates of evolution in the mandible and dentition occur later in amphisbaenians, during the origin of the "acrodont-like" dentition of trogonophids (Fig. 2c). A final example comes from dibamids, which do not have particularly accelerated phenotypic rates in most body regions (Fig. 2a,b,d), also reflected in the global morphological clock (Suppl. Fig. S4), but have fast rates of change in the palate and braincase

(Fig. 2b).

Congruence and conflicts between data types and methods

We compared phenotypic rates of change inferred from phylodynamic approaches with those recovered from phylogenetic comparative methods (PCM) on our GMM dataset—using BayesTraits[39] and RRphylo[40]—two widely implemented approaches in macroevolution over the last decade[12,31,39,55,56]. Our results indicate a drastically different pattern of rate inferences across these different methods and data types that, to our knowledge, have never been previously detected (Figs. 3-5, Suppl. Fig. S5-26).

Overall, clock rates using discrete data from the skull surface result in comparatively slower rates of change relative to PCM approaches with geometric morphometric data (Fig. 3a-f). Besides the difference in rate magnitude, there is also no linear relationship on rate estimates for each node between estimates obtained from clock rates and PCM methods (Fig. 5a,b, Suppl. Fig. S25a,b,d,e). Even among the two PCM methods tested here, some of the rate patterns can be somewhat different from each other (Fig. 3c,e), with only a weak linear relationship between their results (Fig. 5c, Suppl. Fig. S25c,f). These differences thus impact rate-based inferences for their mode of selection (Fig. 3g-i).

More specifically, we find congruence between clock and both PCM estimates only in the snake family Elapidae (Fig. 3g-i, branch 5), all indicating significantly accelerated rates on this branch and strong evidence of directional selection in dorsal skull surface characters and shape. Contrasting results between clock and PCM rates (but still congruent among PCM methods) can be found in the stem of Afrophidia, stem of Scolecophidia, early pleurodontan branches, and early gekkotan branches (Fig. 3 a,c,e, g-i, branches 3, 4, 8, 9). The stem of Afrophidia undergoes strong rate acceleration based on discrete data and clock rates, characteristic of directional selection (Fig. 3g), whereas the same branch undergoes substantially decelerating rates measured from geometric morphometrics and PCM rate inference, characteristic of stabilizing selection (Fig. 3h-i). A similar rate acceleration happens at the stem of Scolecophidia under clock rates (Fig. 3g), but which is nonsignificant under GMM/PCM rates (Fig. 3h-i). Finally, clock rates do not find significant rate changes in early pleurodontan and early gekkotan branches (Fig. 3g), but these are found to undergo significant deceleration under GMM/PCM rates (Fig. 3h-i).

Congruence between results from clock rates and RRphylo only, but different from

BayesTraits, can be found in Dibamidae, and the stem teiioid fossil *Dalinghosaurus* (Fig. 3 g-i, branches 10, 11). Finally, we find many instances of contrasting results among all methods employed, such as in the earliest snake branch, the stem fossil snakes (*Najash* and *Dinilysia*), early Neoanguimorpha branches, early acrodontan branches, and several gymnophthalmid branches (Fig. 3 g-i, branches 1, 2, 6, 7, and 12). These are differences that may represent a conflation of differences in both data type and method performance.

Robustness of rate methods to fossil sub-sampling

In order to assess which factor is driving the inconsistencies in rate inference across methods, we tested the impact of fossil sub-sampling, as performed above for its impact on morphospace (see Methods for details). Although we cannot test for accuracy, which can only be achieved using simulated datasets where the true answer is known a priori—e.g.,[57,58], it can provide an estimate of method robustness to variations in tree size and proportion of fossil inclusion.

Our results indicate that clock rate inferences were the most robust approach to fossil sub-sampling (which also led to changes in total tree size), with similar rate profiles across sampling categories for all morphological partitions (Fig. 4a, Suppl. Fig. S23). Among GMM/PCM methods, using both standard and phylogenetically corrected PCs, RRphylo is somewhat robust to fossil subsampling and tree size (Fig. 4c, Suppl. Fig. S24c,d). In contrast, BayesTraits shows radically different results across different sub-sampling categories (Fig. 4b, Suppl. Fig. S24a,b), suggesting it is quite dependent on fossil sampling and tree size. This much greater variation in results reported by BayesTraits relative to RRphylo and clock rates can also be detected when comparing the overall range of rate values inferred by each method pooled across all clades through different sub-sampling categories (Fig. 5d, Suppl. Fig. S26a,c); this also revealed the presence of strong outliers, especially when sampling is reduced to 0% of fossils (Fig. 5d). The same is observed when comparing each method's output across individual clades and pooled across all taxon sub-sampling categories (Fig. 5e, Suppl. Fig. S26b,d). Finally, these patterns are also observed when plotting rates across all individual tree branches for each category of fossil sub-sampling (Supplementary Figs. S5-S22).

DISCUSSION

We find here a remarkable consistency of phenotypic clock rates inferred across different levels of fossil sampling for multiple subdivisions of the phenotype, and with clock rates consistently more robust than rates of evolution based on phylogenetic comparative methods (PCM). This supports recent simulation-based studies that have revealed a higher accuracy of clock models to infer molecular evolutionary rates compared to alternative approaches in molecular evolution[59] (note that PCM methods were not tested in the simulation study, as these are typically only applied to phenotypic data).

Among PCM approaches, RRphylo is somewhat consistent across subsampling strategies whereas BayesTraits demonstrates substantial volatility of rate inference patterns depending on the proportion of fossil sampling and tree size. Despite such differences between PCM approaches, we still find important areas of agreement between both that make their results more similar to each other than they are to phylodynamic rate inference (Fig. 5). These include at least five important clades (Fig. 3g-i, branches 3, 4, 8, 9), besides an overall similar pattern of rate differences among clades—e.g., despite differences in magnitude, overall mean clade rates follow a similar pattern among clades for PCM methods compared to clock rates (Fig. 5e). Collectively, these findings suggest a strong influence on results due to the nature of the data types used by each approach (discrete data by phylodynamics vs GMM data by PCM), despite several differences in inference procedure and robustness among PCM methods. Our results are in agreement with other studies that have shown how inferring evolutionary mode (e.g., Brownian vs Ornstein-Uhlenbeck models) can be strongly impacted by the proportion of fossil inclusion[60,61] and data type (discrete and continuous traits)[62].

We propose that such discrepancy in phenotypic rates estimated from different datatypes should not be seen as a limitation of available methodologies, but rather as expected as they reflect the distinct ontological nature of each data type and the biological information conveyed by them. For instance, phylogenetic morphological datasets typically include discrete features (i.e., characters) that represent the gain or loss of important anatomical structures or their sub-components (e.g., neomorphisms). They may also capture variation that can be directly or indirectly linked to shape (e.g., characters related to certain structures becoming wider or narrower), color, ecology, among others. For technical reasons, however, the artificial discretization of continuous variation—such as shape data—can introduce important logical

biases in morphological phylogenetics [63], and recent guidelines suggest that morphological datasets should treat continuous variation as such and only categorical features should be coded as discrete characters[63,64]. Hence, morphological datasets following this premise (including ours used herein—see Star+Methods), can be useful to explore rates associated with (mostly) discrete (e.g., neomorphic) character changes. Such changes are linked to the concept of evolutionary novelties in the phenotype—i.e., the origin of new, individuated and quasi-independent phenotypic characters, rather than variations upon preexisting characters[16-18]. Geometric morphometric data on the other hand are, by definition and design, used to quantify continuous variation in shape rather than gains or losses of discrete anatomical structures. These changes in shape can be interpreted as phenotypic innovations (sensu [16-18])—i.e., the refinement of pre-existing structures to better integrate novel aspects of the phenotype into new ecological contexts[16-18].

Embracing this distinction allows us to reconcile the apparently highly discrepant patterns of phenotypic rates of evolution detected here. For instance, an acceleration on the rate of phenotypic novelties associated with the origin of total group Serpentes and Scolecophidia (Fig. 3a,g, branches 1 and 3) is mostly driven by the loss of several skull and limb elements, besides major gains or losses in subcomponents of skull in these branches—see further details in these morphological changes in[34,65,66]. In terms of shape changes, however, these are not significantly different from background rates of evolution. Instead, substantial shape changes associated with rate shifts happen elsewhere, such as in the skull of early fossil snakes (Fig. 3e,i, branch 2). This shows a pattern of accelerated phenotypic refinement in fossil snakes on top of the main (discrete) changes that defined the snake body plan at their origin.

Interestingly, both clock and PCM approaches find a strong mosaic of evolutionary patterns across all snakes, with both strongly accelerating and decelerating rates. This is in stark contrast with recent findings suggesting a "macroevolutionary singularity" of snakes, as a reference to their inferred sustained high rates of evolution across all snakes[9]. It is possible that such difference in results between this and previous studies[9] can be explained by methodological differences. Unfortunately, we could not test for this as the previous study used a new rate statistic[9] that has yet to be implemented in a software package.

In another major squamate group, Scincoidea (with > 2,000 extant species) there are not many substantial discrete changes (i.e., no substantial phenotypic novelties, Fig. 3a,g), but we

detect several independent instances of evolutionary innovation of their skull (Fig. 3e,i). This conclusion is supported by a recent study also finding substantial evolutionary elaboration in this clade[10]. Furthermore, in Dibamidae, a mysteriously long branch of limbless and fossorial squamates, both clock and RRphylo estimate accelerated rates of evolution, thus suggesting substantial phenotypic novelties and innovation occurring jointly in the evolution of this lineage (note that this pattern is contradicted by BayesTraits results, but as illustrated above, this method is less robust to fossil sub-sampling, which might be biasing estimates for dibamids, for which there are no fossils currently known). Finally, in amphisbaenians, there are major discrete changes in their early evolution associated with gains and (mostly) losses of skull elements, as in dibamids and early snakes. However, both PCM methods indicate no substantial shift in skull shape rates in the group, suggesting evolutionary innovation occurred rather gradually within this group compared to the more drastic (early-on) rate shifts detected in dibamids and many snake lineages.

In conclusion, we suggest that fundamental differences in data type are expected to generate discrepant evolutionary patterns (such as phenotypic rates), which can be further exacerbated by the nature and accuracy of the methodologies employed. However, many of such discrepancies may actually capture important differences in biological information carried by distinct data types. Whereas discrete character rates captures variation that is compatible with phenotypic novelties, shape changes provide estimates of refinement (or elaboration) leading to phenotypic innovation—see also[19] for a recent and more restrictive definition of phenotypic elaboration and innovation, defined by the direction of shape change in morphospace. This important (but previously overlooked) conceptual distinction enables a better understanding of the differences observed in evolutionary rate patterns detected here, and which we predict to be common across other study systems outside of squamates. Hence, it raises the necessity for phenotypic rate studies to be self-aware regarding the conclusions that can be drawn with the data at hand, and whether their results produce patterns that are more compatible with phenotypic novelties or innovation.

RESOURCE AVAILABILITY

Lead contact

Requests for further information and resources should be directed to and will be fulfilled by the lead contact, Tiago R. Simões (simoes@princeton.edu).

Materials availability

This study did not generate new unique reagents.

Data and code availability.

- All data, scripts and command blocks are available online as Supplementary Data at NNNNNNNNN
- Updated functions for the R package *BTprocessR* is also available at https://github.com/tiago-simoes/BTprocessR2 and for R package *EvoPhylo* v.0.3.3[20] available at https://github.com/tiago-simoes/EvoPhylo.

ACKNOWLEDGMENTS.

We thank the National Science Foundation (NSF - DEB) for Award # 2323124 to TRS and MCZ/Harvard funding to SEP; and Conselho Nacional de Desenvolvimento Científico e Tecnológico for postdoctoral fellowship #151134/2024-3 to ASB. We also thank F. Burbirnk, D. Kizirian, and L. Vonnahme (AMNH) and J. Hanken and S. Kennedy-Gold (MCZ) for their assistance in accessing specimens.

AUTHOR CONTRIBUTIONS

Conceptualization, T.R.S. and S.E.P.; methodology, T.R.S; investigation, T.R.S. and A.S.B.; resources, T.R.S. and S.E.P..; visualization, T.R.S.; writing – original draft, T.R.S.; writing– review & editing, T.R.S., S.E.P., and A.S.B.

DECLARATION OF INTERESTS

The authors declare no competing interests.

DECLARATION OF GENERATIVE AI AND AI-ASSISTED TECHNOLOGIES IN THE WRITING PROCESS

During the preparation of this work, the authors used ChatGPT to assist on the creation of R code.

SUPPLEMENTAL INFORMATION

Supplemental information can be found online at XXX.

REFERENCES

1. Simpson, G.G. (1953). The Major Features of Evolution (Columbia University Press).
2. Gingerich, P.D. (2019). Rates of evolution: a quantitative synthesis (Cambridge University Press).
3. Simões, T.R., Vernygora, O.V., Caldwell, M.W., and Pierce, S.E. (2020). Megaevolutionary dynamics and the timing of evolutionary innovation in reptiles. Nat. Comm. *11*, 3322. 10.1038/s41467-020-17190-9.
4. Stadler, T., Magnus, C., Vaughan, T., Barido-Sottani, J., Bošková, V., Huisman, J., and Pečerska, J. (2024). Decoding Genomes: From Sequences to Phylodynamics (ETH Zurich). 10.3929/ethz-b-000664449.
5. Heath, T.A., Huelsenbeck, J.P., and Stadler, T. (2014). The fossilized birth–death process for coherent calibration of divergence-time estimates. Proceedings of the National Academy of Sciences *111*, 2957-2966.
6. Wright, A.M., Bapst, D.W., Barido-Sottani, J., and Warnock, R.C. (2022). Integrating Fossil Observations Into Phylogenetics Using the Fossilized Birth–Death Model. Annual Review of Ecology, Evolution, and Systematics *53*.
7. Harmon, L. (2018). Phylogenetic comparative methods: learning from trees (Open Access Publication).
8. Revell, L.J., and Harmon, L.J. (2022). Phylogenetic comparative methods in R (Princeton University Press).
9. Title, P.O., Singhal, S., Grundler, M.C., Costa, G.C., Pyron, R.A., Colston, T.J., Grundler, M.R., Prates, I., Stepanova, N., Jones, M.E.H., et al. (2024). The macroevolutionary singularity of snakes. Science *383*, 918-923. doi:10.1126/science.adh2449.
10. Brennan, I.G., Chapple, D.G., Keogh, J.S., and Donnellan, S. (2024). Evolutionary bursts drive morphological novelty in the world's largest skinks. Current Biology *34*, 3905-3916.e3905. https://doi.org/10.1016/j.cub.2024.07.039.
11. Stubbs, T.L., Benton, M.J., Elsler, A., and Prieto-Márquez, A. (2019). Morphological innovation and the evolution of hadrosaurid dinosaurs. Paleobiology *45*, 347-362. 10.1017/pab.2019.9.

12. Watanabe, A., Fabre, A.-C., Felice, R.N., Maisano, J.A., Müller, J., Herrel, A., and Goswami, A. (2019). Ecomorphological diversification in squamates from conserved pattern of cranial integration. Proceedings of the National Academy of Sciences *116*, 14688-14697.
13. Parins-Fukuchi, C., Stull, G.W., and Smith, S.A. (2021). Phylogenomic conflict coincides with rapid morphological innovation. Proceedings of the National Academy of Sciences *118*, e2023058118. doi:10.1073/pnas.2023058118.
14. Evans, K.M., Larouche, O., Watson, S.-J., Farina, S., Habegger, M.L., and Friedman, M. (2021). Integration drives rapid phenotypic evolution in flatfishes. Proceedings of the National Academy of Sciences *118*, e2101330118. 10.1073/pnas.2101330118.
15. Cooney, C.R., Bright, J.A., Capp, E.J.R., Chira, A.M., Hughes, E.C., Moody, C.J.A., Nouri, L.O., Varley, Z.K., and Thomas, G.H. (2017). Mega-evolutionary dynamics of the adaptive radiation of birds. Nature *542*, 344. 10.1038/nature21074.
16. Wagner, G.P. (2014). Homology, genes, and evolutionary innovation (Princeton University Press).
17. Erwin, D.H. (2015). Extinction–How Life on Earth Nearly Ended 250 Million Years Ago. Updated Edition (Princeton University Press).
18. Erwin, D.H. (2020). The origin of animal body plans: a view from fossil evidence and the regulatory genome. Development *147*, dev182899.
19. Guillerme, T., Bright, J.A., Cooney, C.R., Hughes, E.C., Varley, Z.K., Cooper, N., Beckerman, A.P., and Thomas, G.H. (2023). Innovation and elaboration on the avian tree of life. Science Advances *9*, eadg1641.
20. Simões, T.R., Greifer, N., Barido-Sottani, J., and Pierce, S.E. (2023). EvoPhylo: an R package for pre-and postprocessing of morphological data from relaxed clock Bayesian phylogenetics. Methods Ecol. Evol. *14*, 1981–1993. 10.1111/2041-210X.14128.
21. Baker, J., Meade, A., Pagel, M., and Venditti, C. (2016). Positive phenotypic selection inferred from phylogenies. Biological Journal of the Linnean Society *118*, 95-115. 10.1111/bij.12649.
22. Machado, F.A., Marroig, G., and Hubbe, A. (2022). The pre-eminent role of directional selection in generating extreme morphological change in glyptodonts (Cingulata; Xenarthra). Proceedings of the Royal Society B: Biological Sciences *289*, 20212521.

doi:10.1098/rspb.2021.2521.

23. Rolland, J., Henao-Diaz, L.F., Doebeli, M., Germain, R., Harmon, L.J., Knowles, L.L., Liow, L.H., Mank, J.E., Machac, A., Otto, S.P., et al. (2023). Conceptual and empirical bridges between micro- and macroevolution. Nat. Ecol. Evol. 10.1038/s41559-023-02116-7.

24. De Lisle, S.P., and Svensson, E.I. (2023). Evolutionary change is remarkably time-independent across scales. bioRxiv, 2023.2012. 2002.569704.

25. Sheets, H.D., and Mitchell, C.E. (2001). Uncorrelated change produces the apparent dependence of evolutionary rate on interval. Paleobiology *27*, 429-445.

26. Reijenga, B.R., and Close, R.A. (2024). Apparent timescaling of fossil diversification rates is caused by sampling bias. bioRxiv, 2024.2009. 2011.612481.

27. Simões, T.R., and Pierce, S.E. (2021). Sustained High Rates of Morphological Evolution During the Rise of Tetrapods. Nat. Ecol. Evol. *5*, 1403–1414. 10.1038/s41559-021-01532-x.

28. Simões, T.R., Caldwell, M.W., and Pierce, S.E. (2020). Sphenodontian phylogeny and the impact of model choice in Bayesian morphological clock estimates of divergence times and evolutionary rates. BMC Biology *18*, 191. 10.1186/s12915-020-00901-5.

29. Lee, M.S.Y., Cau, A., Naish, D., and Dyke, G.J. (2014). Sustained miniaturization and anatomical innovation in the dinosaurian ancestors of birds. Science *345*, 562-566.

30. Coombs, E.J., Felice, R.N., Clavel, J., Park, T., Bennion, R.F., Churchill, M., Geisler, J.H., Beatty, B., and Goswami, A. (2022). The tempo of cetacean cranial evolution. Current Biology. https://doi.org/10.1016/j.cub.2022.04.060.

31. Goswami, A., Noirault, E., Coombs, E.J., Clavel, J., Fabre, A.-C., Halliday, T.J.D., Churchill, M., Curtis, A., Watanabe, A., Simmons, N.B., et al. (2022). Attenuated evolution of mammals through the Cenozoic. Science *378*, 377-383. doi:10.1126/science.abm7525.

32. Goswami, A., Noirault, E., Coombs, E.J., Clavel, J., Fabre, A.-C., Halliday, T.J.D., Churchill, M., Curtis, A., Watanabe, A., Simmons, N.B., et al. (2023). Developmental origin underlies evolutionary rate variation across the placental skull. Philosophical Transactions of the Royal Society B: Biological Sciences *378*, 20220083. doi:10.1098/rstb.2022.0083.

33. Ballell, A., Dutel, H., Fabbri, M., Martin-Silverstone, E., Kersley, A., Hammond, C.L., Herrel, A., and Rayfield, E.J. (2024). Ecological drivers of jaw morphological evolution in lepidosaurs. Proceedings of the Royal Society B: Biological Sciences *291*, 20242052. doi:10.1098/rspb.2024.2052.
34. Garberoglio, F.F., Apesteguía, S., Simões, T.R., Palci, A., Gómez, R.O., Nydam, R.L., Larsson, H.C.E., Lee, M.S.Y., and Caldwell, M.W. (2019). New skulls and skeletons of the Cretaceous legged snake *Najash*, and the evolution of the modern snake body plan. Science Advances *5*, eaax5833. 10.1126/sciadv.aax5833.
35. Bittencourt, J.S., Simões, T.R., Caldwell, M.W., and Langer, M.C. (2020). Discovery of the oldest South American fossil lizard illustrates the cosmopolitanism of early South American squamates. Communications Biology *3*, 201. 10.1038/s42003-020-0926-0.
36. Martínez, R.N., Simões, T.R., Sobral, G., and Apesteguía, S. (2021). A Triassic stem lepidosaur illuminates the origin of lizard-like reptiles. Nature *597*, 235–238. 10.1038/s41586-021-03834-3.
37. Griffiths, E.F., Ford, D.P., Benson, R.B.J., and Evans, S.E. (2021). New information on the Jurassic lepidosauromorph *Marmoretta oxoniensis*. Papers in Palaeontology *n/a*. https://doi.org/10.1002/spp2.1400.
38. Simões, T.R., Caldwell, M.W., Tałanda, M., Bernardi, M., Palci, A., Vernygora, O., Bernardini, F., Mancini, L., and Nydam, R.L. (2018). The origin of squamates revealed by a Middle Triassic lizard from the Italian Alps. Nature *557*, 706-709. 10.1038/s41586-018-0093-3.
39. Pagel, M., O'Donovan, C., and Meade, A. (2022). General statistical model shows that macroevolutionary patterns and processes are consistent with Darwinian gradualism. Nat. Comm. *13*, 1113. 10.1038/s41467-022-28595-z.
40. Castiglione, S., Tesone, G., Piccolo, M., Melchionna, M., Mondanaro, A., Serio, C., Di Febbraro, M., and Raia, P. (2018). A new method for testing evolutionary rate variation and shifts in phenotypic evolution. Methods Ecol. Evol. *9*, 974-983.
41. Brownstein, C.D., Simões, T.R., Caldwell, M.W., Lee, M.S., Meyer, D.L., and Scarpetta, S.G. (2023). The affinities of the Late Triassic *Cryptovaranoides* and the age of crown squamates. Royal Soc. Open Sci. *10*, 230968. 10.1098/rsos.230968.
42. Singhal, S., Colston, T.J., Grundler, M., Smith, S.A., Costa, G.C., Colli, G.R., Moritz,

C.C., Pyron, R.A., and Rabosky, D.L. (2021). Congruence and conflict in the higher-level phylogenetics of squamate reptiles: an expanded phylogenomic perspective. Systematic Biology, DOI: 10.1093/sysbio/syaa1054.

43. Portik, D.M., and Wiens, J.J. (2021). Do Alignment and Trimming Methods Matter for Phylogenomic (UCE) Analyses? Systematic Biology *70*, 440-662. 10.1093/sysbio/syaa064.

44. Streicher, J.W., and Wiens, J.J. (2017). Phylogenomic analyses of more than 4000 nuclear loci resolve the origin of snakes among lizard families. Biology Letters *13*. 10.1098/rsbl.2017.0393.

45. Burbrink, F.T., Grazziotin, F.G., Pyron, R.A., Cundall, D., Donnellan, S., Irish, F., Keogh, J.S., Kraus, F., Murphy, R.W., Noonan, B., et al. (2020). Interrogating Genomic-Scale Data for Squamata (Lizards, Snakes, and Amphisbaenians) Shows no Support for Key Traditional Morphological Relationships. Systematic Biology *69*, 502-520. 10.1093/sysbio/syz062.

46. Pyron, R.A. (2017). Novel approaches for phylogenetic inference from morphological data and total-evidence dating in squamate reptiles (lizards, snakes, and amphisbaenians). Systematic Biology *66*, 38-56. 10.1093/sysbio/syw068.

47. Reeder, T.W., Townsend, T.M., Mulcahy, D.G., Noonan, B.P., Wood, P.L., Jr., Sites, J.W., Jr., and Wiens, J.J. (2015). Integrated analyses resolve conflicts over squamate reptile phylogeny and reveal unexpected placements for fossil taxa. PLoS ONE *10*, e0118199. 10.1371/journal.pone.0118199.

48. Tałanda, M., Fernandez, V., Panciroli, E., Evans, S.E., and Benson, R.J. (2022). Synchrotron tomography of a stem lizard elucidates early squamate anatomy. Nature *611*, 99-104. 10.1038/s41586-022-05332-6.

49. Caldwell, M.W., Simões, T.R., Palci, A., Garberoglio, F.F., Reisz, R.R., Lee, M.S.Y., and Nydam, R.L. (2021). *Tetrapodophis amplectus* is not a snake: re-assessment of the osteology, phylogeny and functional morphology of an Early Cretaceous dolichosaurid lizard. Journal of Systematic Palaeontology *19*, 893-952. 10.1080/14772019.2021.1983044.

50. Gauthier, J.A., Kearney, M., Maisano, J.A., Rieppel, O., and Behlke, A.D.B. (2012). Assembling the squamate tree of life: perspectives from the phenotype and the fossil

record. Bull. Peabody Mus. Nat. Hist. *53*, 3-308.
51. Conrad, J.L. (2008). Phylogeny and systematics of Squamata (Reptilia) based on morphology. Bulletin of the American Museum of Natural History *310*, 1-182. 10.1206/310.1.
52. Simões, T.R., and Pyron, R.A. (2021). The Squamate Tree of Life. Bulletin of the Museum of Comparative Zoology *163*, 47-95. 10.3099/0027-4100-163.2.47.
53. Zheng, Y., and Wiens, J.J. (2016). Combining phylogenomic and supermatrix approaches, and a time-calibrated phylogeny for squamate reptiles (lizards and snakes) based on 52 genes and 4162 species. Molecular phylogenetics and evolution *94*, 537-547.
54. Mongiardino Koch, N., Garwood, R.J., and Parry, L.A. (2023). Inaccurate fossil placement does not compromise tip-dated divergence times. Palaeontology *66*, e12680. https://doi.org/10.1111/pala.12680.
55. Pigot, A.L., Sheard, C., Miller, E.T., Bregman, T.P., Freeman, B.G., Roll, U., Seddon, N., Trisos, C.H., Weeks, B.C., and Tobias, J.A. (2020). Macroevolutionary convergence connects morphological form to ecological function in birds. Nat. Ecol. Evol. *4*, 230-239. 10.1038/s41559-019-1070-4.
56. Venditti, C., Meade, A., and Pagel, M. (2011). Multiple routes to mammalian diversity. Nature *479*, 393-396.
57. Vernygora, O.V., Simões, T.R., and Campbell, E.O. (2020). Evaluating the Performance of Probabilistic Algorithms for Phylogenetic Analysis of Big Morphological Datasets: A Simulation Study. Systematic Biology *69*, 1088-1105. 10.1093/sysbio/syaa020.
58. Simões, T.R., Vernygora, O.V., de Medeiros, B.A.S., and Wright, A. (2023). Handling Logical Character Dependency in Phylogenetic Inference: Extensive Performance Testing of Assumptions and Solutions Using Simulated and Empirical Data. Systematic Biology *72*, 662-680. 10.1093/sysbio/syad006.
59. Asar, Y., Sauquet, H., and Ho, S.Y.W. (2023). Evaluating the Accuracy of Methods for Detecting Correlated Rates of Molecular and Morphological Evolution. Systematic Biology *72*, 1337-1356. 10.1093/sysbio/syad055.
60. Gearty, W., Allen, B., Godoy, P.L., and Chiarenza, A.A. (2024). The impact of tip age distribution on reconstructing trait evolution using phylogenetic comparative methods.
61. Slater, G.J., Harmon, L.J., and Alfaro, M.E. (2012). Integrating fossils with molecular

phylogenies improves inference of trait evolution. Evolution: International Journal of Organic Evolution *66*, 3931-3944.

62. Mongiardino Koch, N., Ceccarelli, F.S., Ojanguren-Affilastro, A.A., and Ramírez, M.J. (2017). Discrete and morphometric traits reveal contrasting patterns and processes in the macroevolutionary history of a clade of scorpions. Journal of Evolutionary Biology *30*, 814-825. 10.1111/jeb.13050.

63. Simões, T.R., Caldwell, M.W., Palci, A., and Nydam, R.L. (2017). Giant taxon-character matrices: quality of character constructions remains critical regardless of size. Cladistics *33*, 198-219. 10.1111/cla.12163.

64. Goloboff, P.A., Mattoni, C.I., and Quinteros, A.S. (2006). Continuous characters analyzed as such. Cladistics *22*, 589-601. 10.1111/j.1096-0031.2006.00122.x.

65. Garberoglio, F.F., Gómez, R.O., Simões, T.R., Caldwell, M.W., and Apesteguía, S. (2019). The evolution of the axial skeleton intercentrum system in snakes revealed by new data from the Cretaceous snakes *Dinilysia* and *Najash*. Sci. Rep. *9*, 1276. 10.1038/s41598-018-36979-9.

66. Caldwell, M.W. (2019). The Origin of Snakes: Morphology and the Fossil Record (CRC Press).

67. Katoh, K., and Standley, D.M. (2013). MAFFT Multiple Sequence Alignment Software Version 7: Improvements in Performance and Usability. Molecular Biology and Evolution *30*, 772-780. 10.1093/molbev/mst010.

68. Nguyen, L.-T., Schmidt, H.A., von Haeseler, A., and Minh, B.Q. (2015). IQ-TREE: A Fast and Effective Stochastic Algorithm for Estimating Maximum-Likelihood Phylogenies. Molecular Biology and Evolution *32*, 268-274. 10.1093/molbev/msu300.

69. Stayton, C.T. (2005). Morphological evolution of the lizard skull: a geometric morphometrics survey. Journal of Morphology *263*, 47-59.

70. Da Silva, F.O., Fabre, A.-C., Savriama, Y., Ollonen, J., Mahlow, K., Herrel, A., Müller, J., and Di-Poï, N. (2018). The ecological origins of snakes as revealed by skull evolution. Nat. Comm. *9*, 376. 10.1038/s41467-017-02788-3.

71. Bookstein, F.L. (1997). Morphometric tools for landmark data.

72. Cardini, A. (2016). Lost in the other half: improving accuracy in geometric morphometric analyses of one side of bilaterally symmetric structures. Systematic Biology *65*, 1096-

1106.
73. Rohlf, F.J. (2015). The tps series of software. Hystrix *26*, 9-12.
74. Fedorov, A., Beichel, R., Kalpathy-Cramer, J., Finet, J., Fillion-Robin, J.-C., Pujol, S., Bauer, C., Jennings, D., Fennessy, F., and Sonka, M. (2012). 3D Slicer as an image computing platform for the Quantitative Imaging Network. Magn. Reson. Imaging *30*, 1323-1341.
75. Ronquist, F., Klopfstein, S., Vilhelmsen, L., Schulmeister, S., Murray, D.L., and Rasnitsyn, A.P. (2012). A total-evidence approach to dating with fossils, applied to the early radiation of the Hymenoptera. Systematic Biology *61*, 973-999.
76. Zhang, C., Stadler, T., Klopfstein, S., Heath, T.A., and Ronquist, F. (2016). Total-Evidence Dating under the Fossilized Birth–Death Process. Systematic Biology *65*, 228-249. 10.1093/sysbio/syv080.
77. Höhna, S., Landis, M.J., Heath, T.A., Boussau, B., Lartillot, N., Moore, B.R., Huelsenbeck, J.P., and Ronquist, F. (2016). RevBayes: Bayesian Phylogenetic Inference Using Graphical Models and an Interactive Model-Specification Language. Systematic Biology *65*, 726-736. 10.1093/sysbio/syw021.
78. Lewis, P.O. (2001). A Likelihood Approach to Estimating Phylogeny from Discrete Morphological Character Data. Systematic Biology *50*, 913-925. 10.1080/106351501753462876.
79. Rambaut, A., Suchard, M.A., Xie, D., and Drummond, A.J. (2014). Tracer v1.6.
80. Stadler, T., Kühnert, D., Bonhoeffer, S., and Drummond, A.J. (2013). Birth–death skyline plot reveals temporal changes of epidemic spread in HIV and hepatitis C virus (HCV). Proceedings of the National Academy of Sciences *110*, 228-233.
81. Simões, T.R., and Caldwell, M.W. (2021). Lepidosauromorphs. In Encyclopedia of Geology, 2nd edition, D. Alderton, and S.A. Elias, eds. (Academic Press), pp. 165-174. 10.1016/B978-0-12-409548-9.11844-5.
82. Close, R.A., Benson, R.B.J., Alroy, J., Behrensmeyer, A.K., Benito, J., Carrano, M.T., Cleary, T.J., Dunne, E.M., Mannion, P.D., Uhen, M.D., and Butler, R.J. (2019). Diversity dynamics of Phanerozoic terrestrial tetrapods at the local-community scale. Nat. Ecol. Evol. *3*, 590-597. 10.1038/s41559-019-0811-8.
83. Barido-Sottani, J., van Tiel, N.M.A., Hopkins, M.J., Wright, D.F., Stadler, T., and

Warnock, R.C.M. (2020). Ignoring Fossil Age Uncertainty Leads to Inaccurate Topology and Divergence Time Estimates in Time Calibrated Tree Inference. Frontiers in Ecology and Evolution *8*, 1-13. 10.3389/fevo.2020.00183.

84. Zhang, C. (2021). Selecting and averaging relaxed clock models in Bayesian tip dating of Mesozoic birds. Paleobiology *48*, 340-352. 10.1017/pab.2021.42.

85. Xie, W., Lewis, P.O., Fan, Y., Kuo, L., and Chen, M.-H. (2011). Improving marginal likelihood estimation for Bayesian phylogenetic model selection. Systematic biology *60*, 150-160.

86. Kass, R.E., and Raftery, A.E. (1995). Bayes factors. J. Am. Stat. Assoc. *90*, 773-795.

87. Adams, D.C., Collyer, M., Kaliontzopoulou, A., and Sherratt, E. (2016). Geomorph: Software for geometric morphometric analyses.

88. Collyer, M.L., Baken, E.K., and Adams, D.C. (2022). A standardized effect size for evaluating and comparing the strength of phylogenetic signal. Methods Ecol. Evol. *13*, 367-382.

89. Revell, L.J. (2012). phytools: an R package for phylogenetic comparative biology (and other things). Methods Ecol. Evol. *3*, 217-223. 10.1111/j.2041-210X.2011.00169.x.

90. Felice, R.N., and Goswami, A. (2018). Developmental origins of mosaic evolution in the avian cranium. Proceedings of the National Academy of Sciences *115*, 555-560.

91. Burtner, A.E., M. Grossnickle, D., Santana, S.E., and Law, C.J. (2024). Gliding toward an understanding of the origin of flight in bats. PeerJ *12*, e17824. 10.7717/peerj.17824.

92. Anderson, P.S.L., Friedman, M., and Ruta, M. (2013). Late to the Table: Diversification of Tetrapod Mandibular Biomechanics Lagged Behind the Evolution of Terrestriality. Integrative and Comparative Biology. 10.1093/icb/ict006.

93. Arbour, J.H., Curtis, A.A., and Santana, S.E. (2019). Signatures of echolocation and dietary ecology in the adaptive evolution of skull shape in bats. Nat. Comm. *10*, 2036. 10.1038/s41467-019-09951-y.

94. Guangchuang, Y. (2020). Using ggtree to visualize data on tree-like structures. Current Protocols in Bioinformatics *69*, e96. 10.1002/cpbi.96.

KEY RESOURCES TABLE

REAGENT or RESOURCE	SOURCE	IDENTIFIER
Biological samples		
Specimen list with metadata: morphological and molecular	this study (online); Supplementary Tables S1-S7	https://dataverse.harvard.edu/api/access/datafile/10838345
Deposited data		
Supplementary Tables with PCA results	this study (online); Supplementary Tables S8-S37	https://dataverse.harvard.edu/api/access/datafile/10838345
Supplementary Tables with summary statistics results	this study (online); Supplementary Tables S38-S44	https://dataverse.harvard.edu/api/access/datafile/10838345
Supplementary Figures	this study (online); Supplementary Information	Supplementary Information
Output files of phylodynamic and PCM analyses	this study (online)	https://dataverse.harvard.edu/api/access/datafile/10843419
Software and algorithms		
R v. 4.2.1	R Core Team	https://www.r-project.org/
R package *geomorph v. 4.0.8* [83]	CRAN	https://cran.r-project.org/
R package *phytools v. 2.3-0*[85]	CRAN	https://cran.r-project.org/
R package *RRphylo* v. 2.8.1[48].	CRAN	https://cran.r-project.org/
R package *BTprocessR2*	github	https://github.com/tiago-simoes/BTprocessR2
R package *EvoPhylo* v.0.3.3[20]	github	https://github.com/tiago-simoes/EvoPhylo
BayesTraits v. 4.1.1 [47]	BayesTraits website	https://www.evolution.reading.ac.uk/BayesTraitsV4.1.3/BayesTraitsV4.1.3.html
Mr, Bayes 3.2.7* (*developer's version)[55,73]	github	https://github.com/NBISweden/MrBayes
3D Slicer v. 5.2.2[72]	3D Slicer image computing platform	https://www.slicer.org/

EXPERIMENTAL MODEL AND STUDY PARTICIPANT DETAILS

Morphological phylogenetic data.

Morphological data consists of a considerable expansion of the diapsid-lepidosaur dataset of Simões *et al.* [38], which was later expanded especially in number of taxa (up to 145 species) by multiple studies—e.g., [3,34-37]. Most recently, this dataset was reconfigured as a lepidosaur-only dataset and with increased sample of stem squamates [41], totaling 101 (95 lepidosaurs and 6 non-lepidosaurian outgroups). The present morphological dataset was built by first using this last iteration [41] as a starting point for a substantial increase in the sampling of both characters and taxa across extant and fossil squamates with the goal of building a squamate focused dataset. Specifically, we added 63 additional squamates (both fossil and extant), totaling 164 species: 95 extant squamates, 48 fossil squamates, 12 sphenodontians (including the single extant *Sphenodon punctatus*), and nine stem lepidosaurs and non-lepidosaurian reptiles—sampled taxa and accession numbers for morphological data are provided in Supplementary Table S1.

We used a relatively large number of non-squamatan species (21 taxa) to break the exceptionally long (240myr) branch between the only living outgroup (*Sphenodon punctatus*) and squamates. Substantial revisions of characters used in this dataset and applicable across lepidosaurs were performed by Brownstein *et al.* [41], totaling 325 characters therein. Here, we expanded the sampling of characters that are variable across squamates given the expanded taxonomic sampling here by adding 69 characters, totaling 394 characters scored for all 164 taxa. This followed character construction guidelines, such as utilization of contingent coding schemes and homology assessment to avoid logical and biological biases in character construction, or artificial splitting of continuous traits [58,63]. Importantly, here we provide 180 detailed character illustrations for easy reproducibility of character scoring for this dataset.

Molecular phylogenetic data.

Molecular data for total evidence dating (TED) analyses and relaxed clock inference must necessarily consist of a small number of molecular loci due to the exceptionally demanding computing requirements of such inferences. Here, we focused on molecular loci that yield a species tree consistent with much larger phylogenomic datasets—e.g., [30-32,39] —but matching our morphological taxon sample and also small enough for TED.

As a result, we sampled 11 genetic markers (eight nDNA, two mDNA, and one rRNA) for all 95 extant taxa obtained from GenBank (Supplementary Data)— sampled taxa and accession numbers for molecular data are provided in Supplementary Table S2. The sampling was performed to match the morphological data to the species level as much as possible, which was achieved in most cases. In a few instances where species did not match the morphological data, a congeneric taxon was used.

Sequences were aligned in MAFFT 7.490 [67] online server using the global alignment strategy with iterative refinement and consistency scores (G-INS-i). For the protein-coding genes, MAFFT alignments were further verified by translating nucleotide sequences to amino acids and visually inspecting and trimming regions of poor alignment with Geneious Prime (v. 2023.2.1). The final multiple sequence alignment was concatenated for phylogenetic inference, but both concatenated and individual locus alignments are provided as supplementary information. Molecular sequences from all extant taxa were analyzed for the best partitioning scheme and model of evolution using the PartitionFinder algorithm as implemented in IQ-TREE [68] under Akaike information criterion (AIC).

The molecular tree, despite much smaller than existing phylogenomic trees based on various marker types—e.g.,[9,43-45]—, recovers the same overall topology and relationship among major squamate clades as the latter (Supplementary Fig. S28). The only three exceptions are the placement of the homalopsid *Hypsicopus* with the dipsadid *Diadophis*, the gekkonid *Gehyra* within phyllodactylids, and *Gonatodes* not forming a clade with other sphaerodactylids. For these three cases, in the subsequent total evidence analyses we used a topological constraint fixing their placements following the results of Burbrink *et al.* [45] based on AHEs.

Morphological shape data.

There have been few previous studies using high dimensional shape data from geometric morphometrics (GMM) to understand macroevolutionary and macroecological aspects across all major groups of squamates[12,33,69,70]. This includes one study [12] that focused on obtaining 3D data (with several hundred landmarks) on the cranium which provides more shape variables and thus a finer scale resolution of evolutionary changes. However, 3D data imposes a strong limit in the availability of fossil species that can be assessed as fossil vertebrates are rarely preserved in three dimensions and relatively uninformed. This limited the 3D GMM study to a nearly all extant

730 dataset (174 extant and seven fossil species). On the other hand, 2D GMM limits the total
731 number of variables and phenotypic dimensions, but it enables a much larger taxonomic
732 sampling for fossil species, which is especially relevant when addressing deep time
733 macroevolutionary questions. This larger taxonomic sampling thus provides a denser sampling of
734 morphological diversity within and across squamate families, besides better capturing shape
735 variation across important evolutionary transitions by directly including fossil specimens within
736 those transitions.
737 The most extensive study on skull shape evolution across all major groups of squamates
738 using 2D GMM to date [70] included data from 20 homologous landmarks from published
739 photographs, hand drawings, and firsthand obtained photographs and CT scans, culminating in
740 skull samples for 279 extant and 23 fossil species. Despite the large sampling of extant and fossil
741 species using 2D data in Da Silva *et al.* [70] (total = 302 taxa), only 193 were available in their
742 combined evidence phylogenetic tree used to correct for the phylogenetic signal for statistical
743 analyses when including both extant and fossil data [47]. Also, all landmarks were obtained in
744 lateral view of the skull as in a previous study of skull shape change across lizard families [69].
745 However, there is a substantially larger amount of fossil squamates and other lepidosaurs better
746 (or exclusively) preserved in dorsal view (see Supplementary Table S4) and the symmetric
747 nature of the skull bones in dorsal view makes it easier to detect taphonomic distortions, and
748 retro-deform skulls in some instances. Finally, all previous studies have focused on sampling
749 data from within squamates, only sampling a single outgroup species (the modern tuatara,
750 *Sphenodon punctatus*), from the sister lineage to squamates—sphenodontians—which diverged
751 from the squamate branch at ~260 million years ago[3,52].
752 In order to maximize sampling of fossil species for geometric morphometric (GMM)
753 analyses, we opted for the collection of 2D landmark data, since the vast majority of squamate
754 fossils are not preserved in three-dimensional articulation, and those that have 3D preservation,
755 most do not have CT scan data openly available for 3D landmarking. Therefore, 2D landmarking
756 maximizes the collection of observational data points, despite being limited by the number of
757 variables compared to 3D GMM approaches.
758 To assess the best candidate cranial region and aspect of cranial morphology for 2D
759 geometric morphometrics, we conducted a survey of 88 fossil lepidosaur species (including 6
760 non-lepidosaurian outgroups used for all analyses) represented by 272 specimens

761 (Supplementary Table S4). Our results indicate that the skull in dorsal view is the most
762 commonly preserved aspect (dorsal = 75 occurrences, lateral = 48, ventral =45), and that the
763 mandible is far more frequently observed in lateral view than medial view (73 and 51
764 occurrences, respectively). Our personal evaluation also indicated that specimens preserved
765 exclusively in lateral view were frequently more distorted than those preserved only in dorsal
766 view. Therefore, despite previous attempts to quantify squamate skull shape in lateral view using
767 2D GMM [70], we opted here for a new landmark data collection focusing on dorsal view only for
768 maximizing sample size and minimizing distortion.
769 After discarding all duplicates, species not included in the phylogeny (due to phylogenetic
770 instability), and only keeping specimens for which all landmarks could be confidently placed, we
771 obtained a final fossil sampling of 30 fossil lepidosaur species (Suppl. Table S3). These were
772 subsequently removed to test for the impact of reduced fossil sampling on inferences of
773 morphological disparity and rates of evolution. Taxon removal for GMM and shape-based rates
774 of evolution was homogeneous across the phylogeny (e.g., one species removed by family),
775 rather than random, in order to reproduce the sampling strategy of most researchers (i.e.,
776 maximizing diversity of clade representation). This resulted into four categories of taxonomic
777 inclusion: 24.5%, 14%, and 0% of sampled taxa as fossils (Suppl. Table S5).
778 We identified 35 homologous landmarks and 102 semilandmarks (totaling 137 points; see
779 Suppl. Fig. S27 and Supplementary Table S6). Landmarks were partitioned into premaxilla (4
780 landmarks), nasals (5), prefrontals (4), frontals (7), parietal (5), supraoccipital (three),
781 basioccipital (one), quadrates (one), and ectopterygoids (4). They comprise 26 type I landmarks
782 and 9 type II landmarks *sensu* Bookstein [71]. Semilandmarks were placed on the outline of the
783 anterior margin of the premaxilla (14 semilandmarks), around the internal margin of the orbital
784 fossa (22 on each side), and along the lateral margin of the parietal—in snakes, it followed the
785 sagittal crest, when it was pronounced (22 on each side).
786 The ectopterygoid landmarks and semilandmarks in the orbital and supratemporal fossae
787 were included to accommodate the absence of the jugal bar in snakes and amphisbaenians,
788 enabling a unified analysis with non-ophidian squamates. Previous studies excluded landmarks
789 in the jugal region for snakes and created a snake subsample in the dataset [12,70]. Here, we chose
790 to use jugal landmarks and only include landmarks comparable across all squamates without
791 subsampling for specific clades for better among clade comparability. Fossil specimens with

poorly preserved or asymmetric regions were corrected using side reflection. For all other specimens, we followed the recommendation of places landmarks on both sides of the skull to take into account the potential impact of skull asymmetry [72]. Landmarks and semilandmarks were digitized with tpsDig2 v.2.32 and subsampled with tpsUtil v.1.83[73], with semilandmarks spaced equally along curves.

CT scans of living squamates were obtained from MorphoSource and digitally segmented with 3D Slicer v.5.2.2[74] (e.g., to remove osteoderms and soft tissue) and exported in dorsal view using orthographic projection for parallax correction. These were complemented by high resolution photographs of living and extinct squamates in dorsal view, all collected by the same individual (TRS) (Supplementary Table S3).

METHOD DETAILS

Bayesian phylogenetic inference.

Bayesian analysis of the morphological data set was performed using Mr. Bayes developers version (future Mr, Bayes 3.2.8) compiled from source code (available at https://github.com/NBISweden/MrBayes) [75,76] using the Della HPC cluster at Princeton University. The software choice was decided based on the diversity of relaxed clock models available (see further information below) and ability to run analyses on a feasible amount of time. Specifically, the alternative software with a wide range of available clock models, RevBayes[77], would take an order of magnitude longer than Mr. Bayes to run the same analyses (lasting weeks instead of days).

The molecular component of the combined evidence dataset was analyzed under the GTR + gamma model and subdivided into four partitions (see above for partitioning and model testing). For the morphological data, we used the Mkv + gamma substitution model [78] (Mk with ascertainment bias correction). The molecular only dataset was run for 30 million generations, under 4 independent runs with 4 chains each, temperature = 0.007, 25% burn-in, and sample frequency at every 1,000 generations. The total-evidence analyses (using morphological and molecular partitions) used similar parameters but ran over 70 mi generations.

Stationarity was assessed using standard measures, such as average standard deviation of split frequencies (ASDSF < 0.05) and potential scale reduction factors (PSRF ≈ 1 for all

parameters). Effective sample size (ESS) values were assessed using Tracer v.1.6 [79], reaching >200 for all parameters. Our reported summary trees were calculated with standard output tree procedures available in MrBayes: the majority rule consensus tree (MRC) and the maximum compatible tree (MCT).

Phylodynamic relaxed clock Bayesian macroevolutionary analyses.

We implemented total-evidence-dating using the fossilized birth-death tree model (FBD), under relaxed clock models in MrBayes [75,76]. Sampling strategy among extant taxa was set to "diversity" , which is more appropriate when extant taxa are sampled in a way to maximize diversity (as performed herein) and fossils are assumed to be sampled randomly [76]. Given the chronological gap between most species and phylogenetic distance between most taxa— as typical for most total evidence studies of highly diverse groups spending thousands of species— we used a no sampled ancestor model (rho = 1) where all fossils are considered to be tips only, and which can avoid overestimates of divergence times for morphological clocks [28].

Importantly, for our focal analyses we implemented the Skyline FBD model (SFBD), which enables a piecewise constant inference of speciation, extinction, and fossil sampling parameters, which are allowed to vary across time bins [80]. This provides more biologically realistic parameterization of the diversification processes and has been demonstrated to yield more reliable divergence time estimates using empirical data [28,76]. We implemented SFBD with a flat prior (uniform distribution: samples ∈ U[0,1]) on the parameters of relative extinction (= turnover) and probability of sampling fossils, whereas the net diversification rate was sampled from an exponential distribution with mean = 1.0.

All FBD parameters were allowed to shift in the skyline model at four time frames, creating five distinct time bins for parameter sampling, which are large enough to include sufficient lineages to accurately inform FBD parameters and also matching critical events in the history of squamates: i) the Jurassic-Cretaceous boundary (145 Ma), when a shift is typically observed in the fossil record of lepidosaurs, with the drastic decrease in diversity of sphenodontians and an increase in the diversity of squamates [28,81]; ii) the Early-Late Cretaceous boundary (100.5 Ma), which marks the disappearance of several early squamates and the much higher diversity of crown group squamates observed in the Late Cretaceous [81,82]; iii) the Cretaceous-Paleogene boundary (66Ma), which marks the end Cretaceous mass extinction,

allowing us to account for potential shift in speciation and extinction rates of squamates after that event; iv) the Paleogene-Neogene boundary (23Ma), after which modern genera become abundant in the fossil record of squamates [52,81] and potentially correlates with the exponential increase in the number of squamate lineages in the Cenozoic [82], thus accounting for a potential shift of this relatively recent diversification history.

The age of the root (node representing the MRCA of †*Youngina* and crown reptiles) was sampled from an offset exponential distribution with a hard bound for the minimum age (based on the minimum age for †*Youngina*, at 255 Ma) and a soft maximum age, with the mean of the exponential distribution based on a recent TED analysis for this node (280Ma). This provides a relatively low but nonzero probability for sampling ages older than set the maximum age for the root.

The vast majority of our calibrations were based on tip-dating, which accounts for the uncertainty in the placement of fossil taxa and avoids the issue of constraining priors on taxon relationships when implementing bound estimates for node-based age calibrations[75]. The range of the stratigraphic occurrence of the fossils used for tip-dating here were used to inform the uniform prior distributions on the age of those same fossil tips, which avoids biases that can be introduced by point age calibrations on the age of the fossils [83], by using a uniform prior distribution on the age range of the stratigraphic occurrence of the fossils (Supplementary Table S7). Complementary to that, in clades for which we lacked some of the oldest known fossils in our analysis and for which there is overwhelming support in the literature (and in all our other analyses), we employed node age calibrations with a soft minimum age. The single clade node calibration for that is Serpentes: based on †*Eophis underwoodi* (Bathonian, Middle Jurassic—UK) → 168.3-166.1 MYA (166.1,168.3), as in previous studies[3,38,41].

We assessed the fit of various clock models to our data, including a new suit of clock models available in the developer's version of Mr. Bayes, which was compiled from source code (available at https://github.com/NBISweden/MrBayes). These models include the continuous autocorrelated clock model (TK02) and three uncorrelated clock models: the white noise model (former IGR model up to version 3.2.7a of Mr. Bayes) [84], and the new independent gamma rate (IGR) and independent lognormal clock (ILN) models [84]. These models represent radically different interpretations of how and where in the tree evolutionary rates are allowed to change

884 across lineages, which can substantially impact divergence time estimates using morphological
885 and/or molecular data [28,84].

886 We tested model fit using the stepping-stone sampling strategy to assess the marginal
887 model likelihoods [85] and calculated Bayes Factors (BF)—30 steps (+5 as burn in) for 100 million
888 generations. Due to convergence issues for the computationally heavy stepping-stone strategy,
889 we also compared marginal log likelihoods inferred during empirical analyses reported as
890 harmonic means. Using the significance thresholds of Kass and Raftery [86], we found a strong
891 support for the ILN clock model relative to all other models (Table 1), with the autocorrelated
892 TK02 model having by far the weakest support (BF>400) and also with one or multiple
893 independent runs not reaching convergency. Our results thus focused on the output from ILN
894 clocks.
895
896 **Table 1.** Results of clock and tree model fit using marginal log likelihoods for Bayes Factor
897 comparisons. All BF values are reported relative to the best fitting models within each
898 comparable category defined by the total number of free parameters.

Clock Model	Tree Model	Free Parameters	ASDSF	lnL (HM)	BF (HM)	lnL (SS)	BF (SS)
ILN	FBD	25	0.014897	-157162.5	0	-150738.7	0
ILN	SFBD	37	0.01336	-157140.8	0	na	na
WN	FBD	25	0.013349	-157231.7	-69.2	-158251.6	-7512.85
WN	SFBD	37	0.014644	-157226.4	-85.61	na	na
IGR	FBD	25	0.015578	-157211.5	-68.14	-152463.9	-1725.16
IGR	SFBD	37	0.030888	-157482.3	-255.92	na	na
TK02	FBD	25	0.055625	-157612.3	-468.91	-158486.7	-7747.93
TK02	SFBD	37	0.074106	-157638.1	-411.69	na	na

899 Abbreviations: BF, Bayes Factor; HM, harmonic means; LnL, marginal ln-likelihood; SS,
900 stepping-stones.
901

902

903 The starting value for the prior on the clock rate was given an informative prior as per
904 previous non-clock analysis—the median value for tree height in substitutions from posterior
905 trees divided by the age of the tree based on the median of the distribution for the root prior[3,28]
906 (104.45/267.5= 0.3904). The mean of the lognormal distribution was given the value based on
907 the non-clock tree estimate in natural log scale: ln(0.3904) = -0.9404. Finally, we chose a broad
908 standard deviation around the mean ($\sigma = 1.0$).

909 To account for mosaic evolution across the phenotype and to be able to directly compare
910 rates of phenotypic evolution in the skull using phylogenetic and geometric morphometric
911 inference, we partitioned morphological phylogenetic characters following an anatomy-based
912 partitioning scheme. Specifically, we created four partitions, the first one closely matching the
913 same elements (dermal elements of the skull surface) landmarked for GMM, and for which
914 evolutionary rates were extracted for direct comparison with GMM-based rate inference: skull
915 surface dermal bones (characters 1-113, 393, 394), skull palatal bones and braincase (characters
916 114-208); mandibles and dentition (characters 209-275); postcranium (characters 277-392). We
917 did not further subdivide these categories in order to keep a minimum number of characters that
918 are capable of informing branch lengths. Further, the postcranial partition could not be further
919 subdivided (e.g., axial skeleton and limbs) due to the near-complete absence of appendicular
920 skeleton across limb reduced squamates (most notably, snakes), which represent a substantial
921 portion of the data.

922 The prior on the variance of clock rates (informing individual branch rates) was then
923 unlinked between all molecular and morphological partitions, enabling the inference of branch
924 specific rates for each partition. As this is a heavily parameterized analysis, we maximized
925 convergence and sampling of parameters for clock rates by conducting a two-step procedure.
926 First, we performed a completely unconstrained Bayesian evolutionary inference using the best
927 fit models indicated above (e.g., ILN clock and skyline FBD) with only two clock partitions (one
928 morphological and one molecular) for 70 million generations. Secondly, the resulting tree
929 topology from the first step was used to fix the topology of subsequent multi-clock analyses,
930 with all molecular and morphological partitions unlinked, as described above, for another 70
931 million generations. This ensured a large effective sample size and convergence of all parameters
932 despite the large number of tips and complexity of the models implemented.

QUANTIFICATION AND STATISTICAL ANALYSIS

Geometric morphometric analyses.

For each taxon sampling category, we performed separate Generalized Procrustes Analysis (GPA) on the landmark data using the 'gpagen' function in the R package *geomorph* v. 4.0.8 [87]. Principal component analysis (PCA) and phylogenetically corrected PCA (pPCA) were conducted using the 'gm.prcomp' function in *geomorph*. The pPCA utilized generalized least-squares for series ordination to center and to estimate the covariance matrix, with residuals projected onto an orthogonal projection. To access the phylogenetic signal among Procrustes shape variables, we used the 'physignal' and 'physignal.z' functions in *geomorph*, with the last estimating effect size using the "front" method for lambda [88]. Morphospace and phylomorphospace projections (based on the first three pPCs) were performed using the R package *phytools* v. 2.3-0[89] with the 'phylomorphospace' and 'contMap' functions.

Skull shape evolutionary rates.

Prior studies have used phylogenetically-corrected principal components (pPCs) for subsequent evolutionary mode or rate inference [12,31,90], or standard PCA [91,92], or both [15,93]. Here we have done both. We used the standard principal components (PCs) representing 95% of variance in skull shape data (38, 41, and 44 highest ranking PCs) and the phylogenetically corrected principal components (pPCs) representing 95% of non-phylogenetic residual variance of skull shape data (40, 43 and 45 highest ranking pPCs) to calculate rates of phenotype evolution. All inferences used the MCT tree obtained from relaxed clock Bayesian inference (the same used preferred clock rates of evolution) the PCs/pPC residuals were used as inputs for shape rate estimates using BayesTraits v. 4.1.1 [39] and the R package *RRphylo* v. 2.8.1[40].

For BayesTraits, we used the variable rates model of evolution, which assumes a Brownian motion model of rate change across the tree while also allowing for rate shifts across branches, with the number and location of rate shift being inferred with reversible jump MCMC[56]. It also performs branch transformations to detect the overall mode of trait evolution, using parameters delta (e.g., early burst vs late mode of rate of acceleration), kappa (punctuated mode with rates concentrated on speciation events), and lambda (where rates better fit the

phylogenetic structure of the input tree). For this dataset, we used 200 million generations, sampling at every 20,000 generations and a burn-in of 25% (50M generations), using 2 independent runs.

Parameters values across independent runs were assessed using Tracer v.1.6 [79], which indicated stationarity and convergence across runs, with an effective sample size (ESS) values reaching >200 for all parameters. Summary statistics and mapping of rates across the tree were conducted using a modified version of functions formally available in the discontinued R package *BTprocessR* — we updated these functions and made them all available again in GitHub: https://github.com/tiago-simoes/BTprocessR2. We used the function 'rjpp' to postprocess the posterior parameter values and posterior trees and generate summary statistics for all posterior parameters. This was followed by mapping inferred mean rate changes across the MCT tree using the *ggtree* R package [94].

Skull shape evolution rates were also assessed with the *RRphylo* R package, using yhe function RRphylo0, which uses phylogenetic ridge regression to infer ancestral states for each internal node and calculate rates of evolution. It provides a complementary approach to BayesTraits to test for evolutionary rates taking into account multivariate data types and non-ultrametric trees [40]. Differently from BayesTraits and clock rates, this is a deterministic approach, and multiple input trees are recommended to account for phylogenetic uncertainty. However, for purposes of comparability across methods, we used the same input time calibrated tree as used for BayesTraits and clock rate inferences.

Figures and Captions

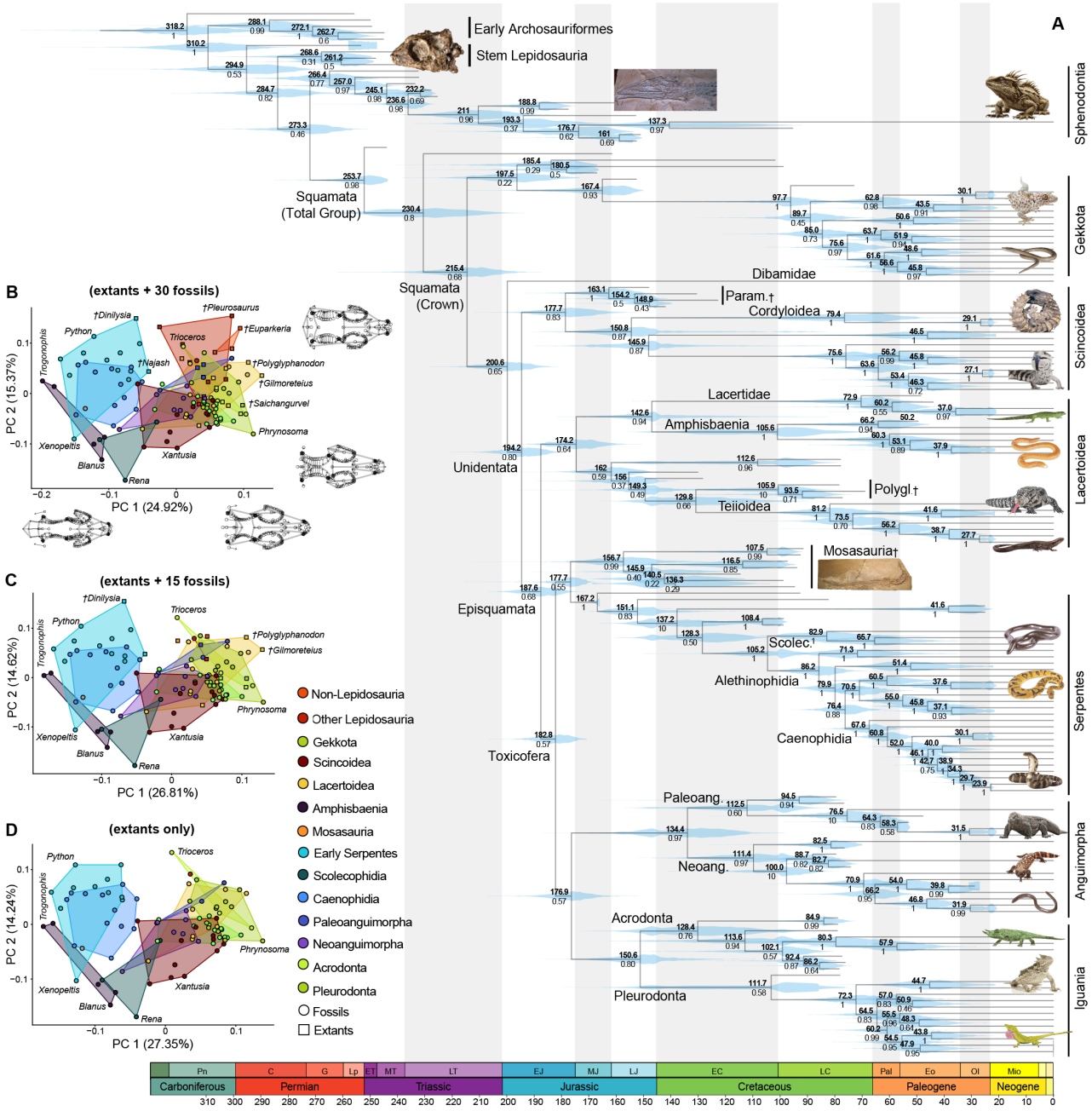

Fig. 1. New total evidence dating time-tree of squamates (and other lepidosaurs) and impact of fossil sampling in morphospace patterns. A, times inferred from relaxed clock phylodynamic inference for all morphological characters ("global clock") using full dataset (164 species). Node violin plots indicate 95% HPD divergence times. Values on nodes indicate mean divergence times (top, in bold), and posterior probabilities (bottom)**. B**, morphospace using 122 species (all extants + 30 fossils; 24.5% of fossil sampling) based on PC 1 vs PC2 and skull shape plots indicate direction of skull shape change along PC axes. **C**, morphospace using 106 species (all extants + 15

997 fossils; 14% of fossil sampling) based on PC 1 vs PC2. **D**, morphospace using 92 species (all extants + 0
998 fossils; 0% of fossil sampling) based on PC 1 vs PC2. Some regions of the morphospace are occupied
999 almost exclusively by completely extinct lineages (e.g., upper right by fossil sphenodontians). Further,
1000 morphospace limits for some crown squamate families are represented by fossils (e.g.,
1001 polyglyphanodontians among lacertoids, in yellow; stem fossil snakes among early snakes
1002 ("Haenophidia"), in cyan). Iterative fossil removal contracts crown clade morphospaces, although the
1003 relative positions and overlap are mostly unchanged. For additional results depicting the same changes
1004 across PC1 vs PC3 and PC2 vs PC3, see Suppl. Fig. S3.
1005

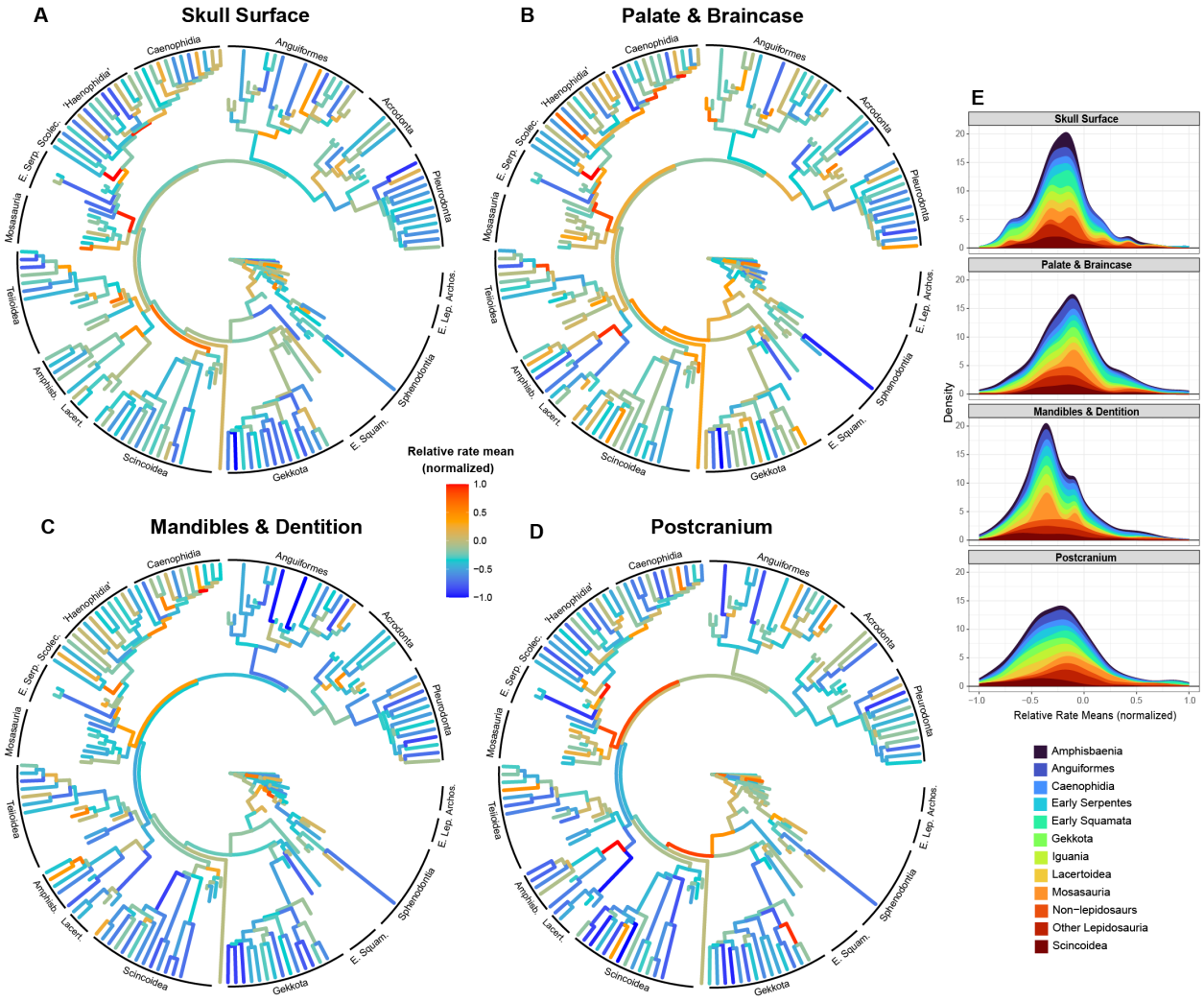

Fig. 2. Relaxed clock phylodynamic inference for four morphological character partitions across lepidosaurs using full dataset (164 species). Topology constrained to global clock phylodynamic tree (Fig. 1a) with all rates normalized. **A**, skull surface partition rates. **B**, palate and braincase partition rates. **C**, mandibles and dentition partition rates. **D**, postcranial partition rates. **E**, histogram of clock rates by partition and clade. Note the strong difference in rate values on equivalent branches of the tree depending on the morphological partition. Also, overall slower rates for mandibles, dentition and postcranial characters relative to skull surface, palate and braincase. For rates values for all partitions combined (global clock rates), see Suppl. Fig. S4, and with fossil subsampling, see Suppl. Fig. S5-7.

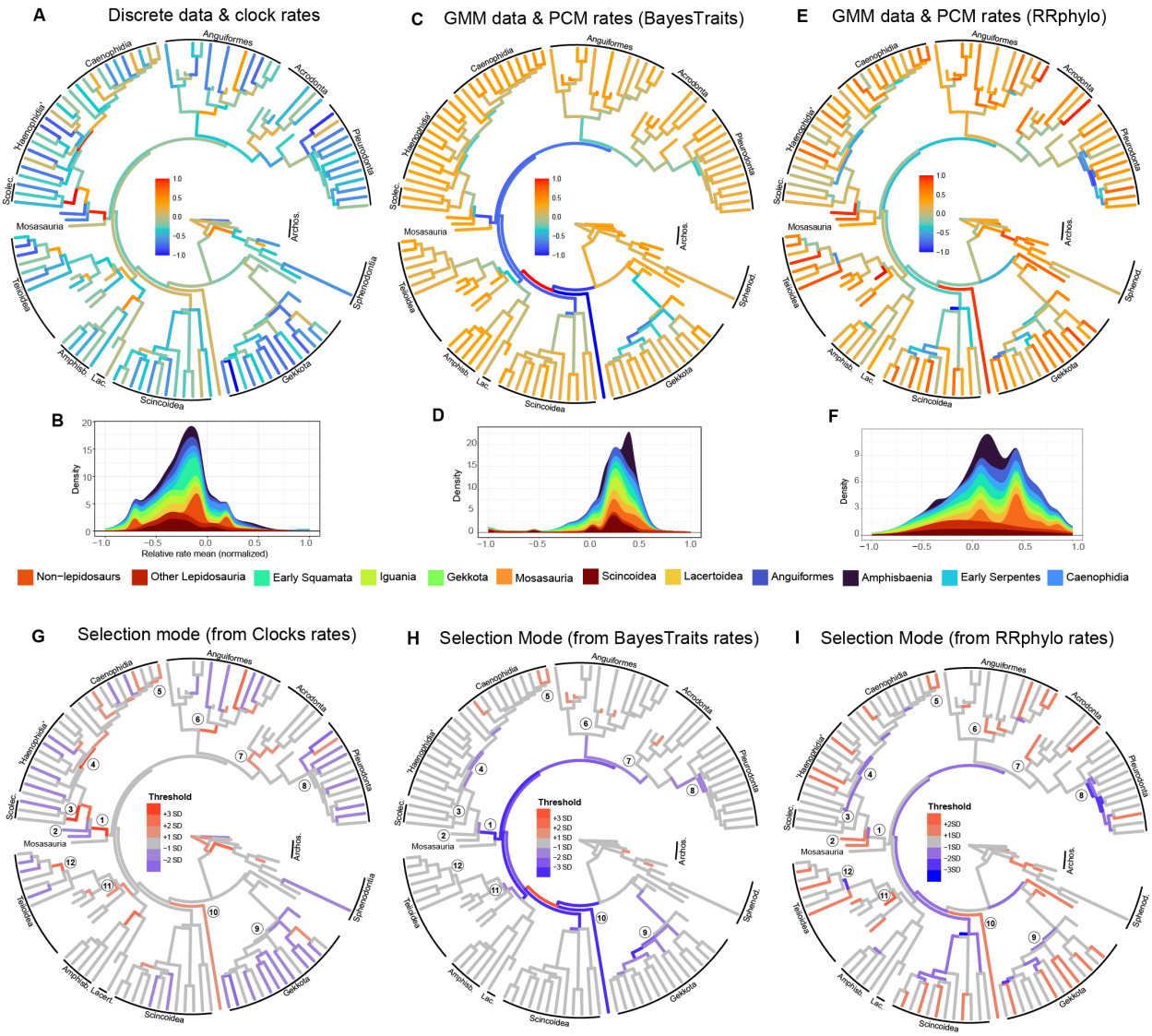

Fig. 3. Evolutionary rates estimate comparison for skull surface data across inference methods. A, relaxed clock phylodynamic inference using discrete characters. **B,** histogram of clock rates by clade. **C,** BayesTraits rates using geometric morphometric (shape) data based on phyloPCs representing 95% of total variation. **D,** histogram of BayesTraits rates by clade. **E,** RRphylo rates using geometric morphometric (shape) data based on phyloPCs representing 95% of total variation. **F,** histogram of RRphylo rates by clade. **G**, selection mode inferred from clock rates. **H**, selection mode inferred from BayesTraits rates. **I,** selection mode inferred from RRphylo rates. Node numbers in g-i represent the following focus branches: 1, earliest snake branch; 2, early fossil snakes; 3, stem of Scolecophidia; 4, stem of Afrophidia; 5, Elapidae; 6, stem of Neoanguimorpha; 7, stem of Acrodonta; 8, early Pleurodonta; 9, early Gekkota; 10, Dibamidae; 11, Dalinghosaurus; 12, Gymnophtalmidae. All rates mapped on the same time-calibrated evolutionary tree of sample size = 122 species (30 fossils; 24.5% fossil sampling). Rate values inferred from GMM data are on average higher than using discrete character data, despite substantial differences in the pattern of rate distributions among branches (see also Fig. 4). For additional

rates mapped on trees across different sample sizes, and using both phyloPCs and standard PCs, see Supplementary Figs. S8-S22.

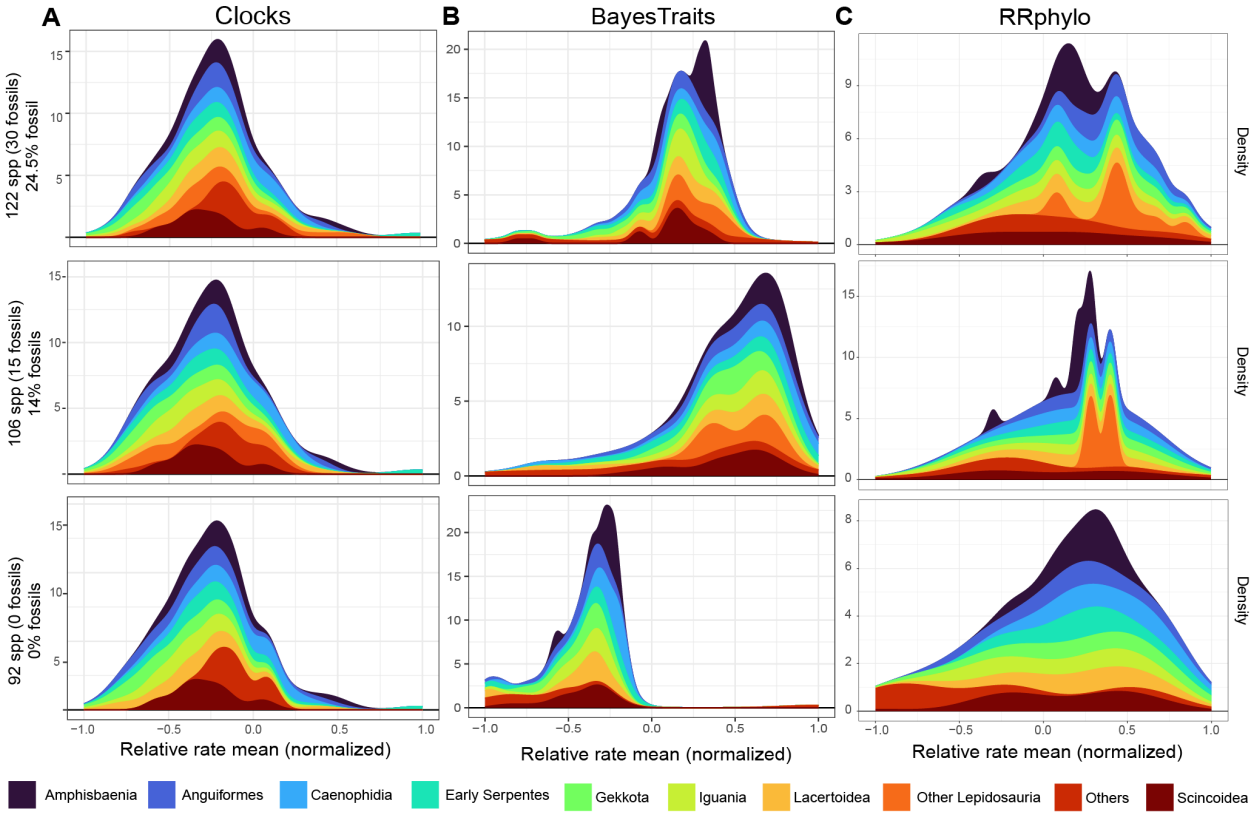

Fig. 4. Rate distributions by clade across methods and fossil sampling efforts. A, histogram of clock rates by clade. **B,** histogram of BayesTraits rates by clade. **C,** histogram of RRphylo rates by clade. Top row represents full taxon sampling matching GMM data set (122 taxa, 24.5% being fossils), middle row represents taxon sampling matching GMM data set with 50% of fossils removed (106 taxa, 14% being fossils), and bottom row represents taxon sampling matching GMM data set with all fossils removed (92 taxa, 0% being fossils). For clock rate distributions for each partition and fossil subsampling category, see Suppl. Fig. S23. For PCM rate distributions for each method contrasting standard and phylogenetically corrected PCs, see Suppl. Fig. S24.

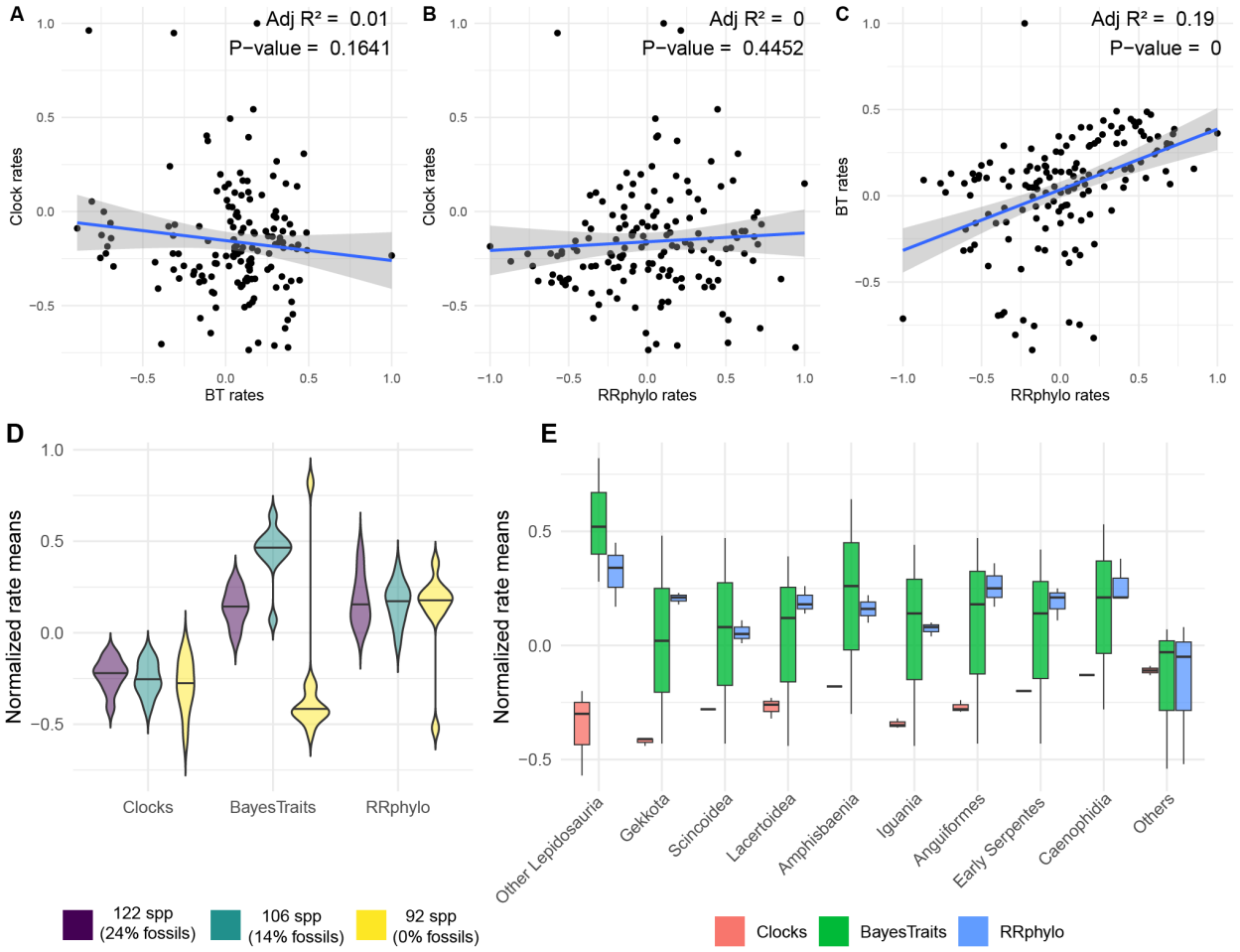

Fig. 5. Comparison of rate inferences across methods and fossil sampling efforts. A, linear regressions between clock and BayesTraits normalized rates. **B**, linear regressions between clock and RRphylo normalized rates. **C**, linear regressions between BayesTraits and RRphylo normalized rates. **D**, violin plot of normalized rate distributions by method and three fossil sampling strategies (pooled across all clades). **E**, box plots of normalized rate distributions for each major clade (pooled across all fossil sampling strategies). There is no detectable correlation on a node-by-node comparison between clock rates and rates using phylogenetic comparative methods (PCMs). However, there is some (although week) correspondence between the two PCM approaches using GMM data (BayesTraits and RRphylo in **c**) with disparity of rate values using BayesTraits being much higher than either clocks or RRphylo, for all clades analyzed separately or together and regardless of fossil sampling effort (in **D** and **E**). All PCM rates here used phyloPCs (see Suppl. Fig. S25 and S27 for similar results using standard PCs.)